New Insight into CO Photodesorption from C-60

ARTICLE *in* THE JOURNAL OF PHYSICAL CHEMISTRY A · JULY 2012

Impact Factor: 2.69 · DOI: 10.1021/jp305133z · Source: PubMed

2 AUTHORS:

Jan Mitschker
Carl von Ossietzky Universität Oldenburg
4 PUBLICATIONS **4** CITATIONS
SEE PROFILE

Thorsten Klüner
Carl von Ossietzky Universität Oldenburg
119 PUBLICATIONS **1,515** CITATIONS
SEE PROFILE

THE JOURNAL OF PHYSICAL CHEMISTRY A

Article

pubs.acs.org/JPCA

New Insight into CO Photodesorption from C_{60}

Jan Mitschker and Thorsten Klüner*

Institute of Pure and Applied Chemistry, Theoretical Chemistry, Carl von Ossietzky Universität Oldenburg, Carl-von-Ossietzky Straße 9-11, 26129 Oldenburg, Germany

ABSTRACT: We report on new results concerning the interaction of CO with C_{60} in the electronic ground state and an electronically excited state. We found that the energetically most favorable geometries are vertical or horizontal in the ground state but in the excited state the molecule is tilted by about 40°. The two-dimensional potential energy surfaces of these states were used to simulate the photodesorption process induced by a short laser-pulse. An interesting desorption mechanism was found, leading to a bimodal velocity distribution for each rotational quantum state if the molecule starts from the rovibronic ground state.

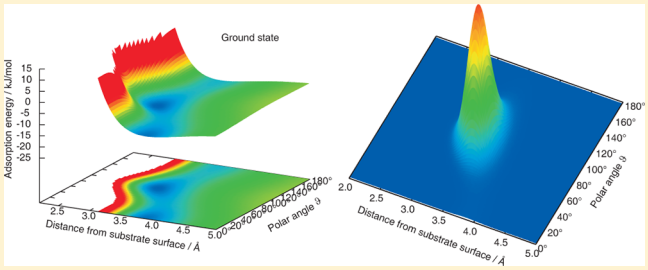

INTRODUCTION

The combination of ab initio quantum mechanical and quantum dynamical calculations is still a challenging task even for simple systems, and especially for photochemical processes that include electronically excited states. One of the most simple reactions is photodesorption of small molecules from surfaces. This process is a prototype of nonadiabatic surface reactions and is very important in photocatalysis. It is a first step toward a detailed understanding of more sophisticated processes like vibrational and rotational excitation or bond forming and bond breaking, especially photodissociation. Furthermore, photodesorption may be important for molecular switches, rotors or machines as well.[1]

The photodesorption of diatomic molecules from metal oxide surfaces has been studied extensively in our group.[2−8] In this paper we will consider the photodesorption of CO from a *single* C_{60} molecule. This fullerene offers a large surface but is still a molecular system, making complicated modeling like embedding unnecessary. Only a few ab initio studies for the adsorption of small molecules on this interesting surface exist.[9] Recently, we reported on first results concerning the adsorption and photodesorption in a one-dimensional case study.[10] Here, we extend our calculations to a two-dimensional case that is physically more realistic. Photoreactions on fullerenes can play an important role in interstellar medium[11] and the adsorption of CO is important for catalysts involving fullerenes.[12] Many applications, for example gas sensors, optical and electronic devices, chromatography materials or coatings have been proposed.[13] Examples of photocatalytic activity are the decomposition of water and oxalic acid.[14] There is a growing interest in this field of chemistry but fundamental steps are still unknown.

The rest of this paper is organized as follows: In the next section we will introduce our quantum chemical and quantum dynamical methods. Then, calculations of the adsorption site will we presented. Hereby, an internal standard will be defined that is used to validate smaller model systems. The calculations are extended to two-dimensional potential energy surface for the ground and one electronically excited state. Finally, quantum dynamical studies are performed that describe the photodesorption.

THEORETICAL METHODS

Methods and Model System. The system consists of only one C_{60} fullerene and one adsorbed CO molecule. Therefore, the formation of C_{60} films, as indicated by experiments, is not considered here. The orientation of the adsorbate is described by three Cartesian coordinates (X, Y, Z) for the translation of the center of mass of the adsorbate and three internal degrees (ϑ, ϕ, r), giving in total the six degrees of freedom of a diatomic molecule. The coordinate system is sketched in Figure 1.

This choice is advantageous because the study can easily be restricted to a smaller number of degrees of freedom and the Hamiltonian in the quantum dynamical treatment does not contain any mixed derivatives. Our study is based on the Born−Oppenheimer approximation. Therefore, in a first step the potential energy surfaces are calculated as a solution of the electronic Schrödinger equation for different nuclear configurations. For the electronic ground state, the ab initio potential energy surface was calculated on the Hartree−Fock level of theory with the molcas program package.[15] Dynamical correlation effects were included by Møller−Plesset second-order perturbation theory (MP2). For the electronically excited state, the complete active space self-consistent field (CASSCF) approach[16] with a subsequent perturbation treatment[17] (CASPT2) was applied. Here, active orbitals are selected with

Special Issue: Jörn Manz Festschrift

Received: May 26, 2012
Revised: July 6, 2012
Published: July 6, 2012

   dx.doi.org/10.1021/jp305133z | J. Phys. Chem. A 2012, 116, 11211−11218

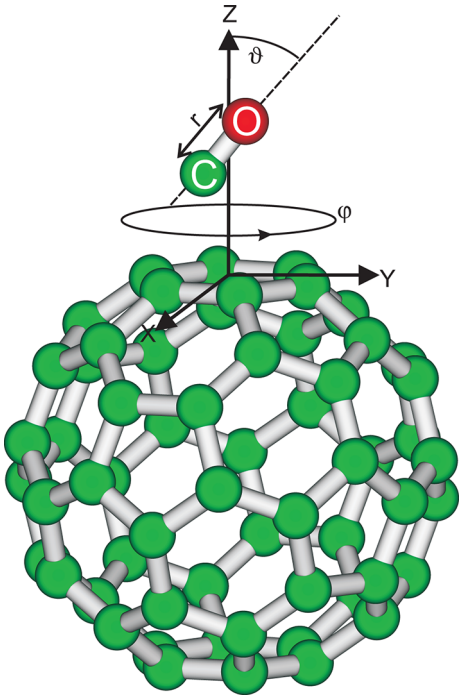

Figure 1. Adsorption of CO on C_{60} with coordinate system inscribed.

occupation numbers that are not restricted to zero or two and which therefore allow well-defined excited states. Dunning's correlation consistent basis sets of various quality were used for the substrate.[18] However, for the adsorbate the triple-ζ basis set has always been applied to obtain correct adsorption and excitation energies. It should be noted that increasing the quality of the basis influences the computational costs dramatically, because going from cc-pVDZ to cc-pVTZ the number of basis functions for each atom doubles. As the interaction is quite weak, the potential energy surfaces are corrected for the basis set superposition error (BSSE) according to the formula by Boys and Bernardi.[19] It was assumed that surface and adsorbate do not change their geometry during the adsorption, and the adsorption energy is therefore given by the equation

$$E_{\mathrm{Ads}} = E_{\mathrm{CO-C_{60}}} - (E_{\mathrm{CO}}^{\{\mathrm{CO-C_{60}}\}} + E_{\mathrm{C_{60}}}^{\{\mathrm{CO-C_{60}}\}}) \quad (1)$$

where the superscript denotes the whole basis set of both molecules. Consequently, for each point of the potential energy surface three single point calculations were necessary.

The quantum dynamical simulations are based on Gadzuk's jumping wave packet approach.[20] The time evolution of a wave packet can be formulated as in eq 2, where a starting wave packet $\Psi(0)$ is propagated for some time τ_n and $t - \tau_n$ in the excited and ground state, respectively. $\hat{H}_{\mathrm{gs}}$ and $\hat{H}_{\mathrm{es}}$ denote the corresponding Hamiltonians of the ground and excited state. Note that the desorption scenario is treated as a completely quantum mechanical process.

$$|\Psi(t;\tau_n)\rangle = \mathrm{e}_{\mathrm{gs}}^{-\mathrm{i}\hat{H}_{\mathrm{gs}}(t-\tau_n)} \cdot \mathrm{e}_{\mathrm{es}}^{-\mathrm{i}\hat{H}_{\mathrm{es}}(\tau_n)} |\Psi(0)\rangle \quad (2)$$

Two different desorption scenarios have been developed for one-dimensional studies. The first one named MGR[21] implies a repulsive excited state. Here, the wave packet is accelerated away from the surface and a high velocity results, which leads to desorption even after relaxation to the electronic ground state. In contrast the Antoniewicz mechanism[22] implies an attractive excited state with shorter equilibrium distances. Now, the wave packet is first accelerated toward the surface but then relaxes into the strongly repulsive area of the electronic ground state. As a consequence, a pronounced acceleration results. It should be noted that these mechanism cover only one-dimensional cases and can be much more complicated for higher dimensional studies.

Within the jumping wave packet approach, the wave packet of the electronic ground state is vertically transferred to the excited state and is propagated for many different residence times τ_n. Then, each quantum trajectory is vertically transferred back to the ground state potential and propagated until the results converge. Because the population of the excited state depletes exponentially, the results of N trajectories are averaged at time t according to

$$\langle \hat{A}(t;\tau) \rangle = \frac{\sum_{n=1}^{N} \langle \hat{A}(t;\tau_n) \rangle \cdot \exp(-\tau_n/\tau)}{\sum_{n=1}^{N} \exp(-\tau_n/\tau)} \quad (3)$$

Here, $\hat{A}$ is the operator corresponding to observable A under consideration and τ is a parameter (resonance lifetime) that corresponds to the spectroscopic lifetime of the excited state. It has been shown that this procedure is equivalent to a solution of the Liouville–von Neumann equation.[1,23] To avoid a large grid in coordinate space, the wave packet is only propagated in reciprocal space at large distances where the potential is actually zero. This grid change method has been proposed by Heather and Metiu.[24] The fraction of the wave packet in this asymptotic region can be considered as desorbed, and therefore the desorption probability is just the norm on this grid, following

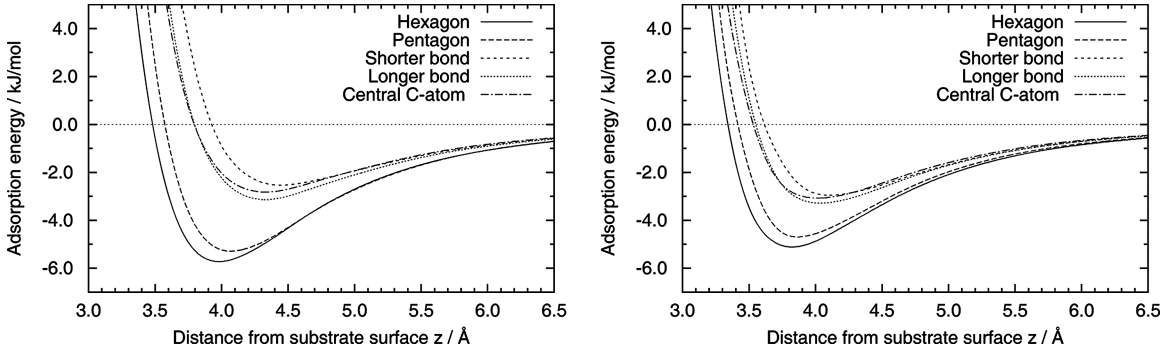

Figure 2. Calculated adsorption energies for different adsorption sites on MP2-level and cc-pVDZ basis with carbon atom (left) and oxygen atom (right) pointing toward the surface. The distances refer to the center of mass of the CO molecule.

dx.doi.org/10.1021/jp305133z | J. Phys. Chem. A 2012, 116, 11211–11218

from eq 3 for $\hat{A} = \hat{1}$. The quantum dynamical simulations were performed with our own program dyn5d and the very efficient split-propagator[25] was applied. For generating the initial wave packet, we propagated a Gaussian wave packet in imaginary time[26] to obtain the rovibrational ground state wave function of the electronic ground state.

RESULTS

C_{60} Geometry. According to our MP2 calculation with a cc-pVTZ basis set, the bond lengths in a single C_{60} molecule with I_h symmetry are 1.443 and 1.404 Å, respectively. The longer bond corresponds to the five-membered rings only but both occur alternately in the six-membered rings. These values have been obtained with the Gaussian03 program[27] and are used throughout the rest of this work. On HF level the latter is 1.369 Å whereas the former does not change. DFT with the B3LYP functional gives a value of 1.389 Å. Experimentally, values of 1.458(6) Å and 1.401(10) Å have been obtained in the gas phase.[28]

For the CO molecule we used an interatomic distance of 1.14 Å, which was kept fixed throughout the study.

Comparison of Adsorption Sites. On a fullerene a few highly symmetric adsorption sites can be identified: The hexagonal and pentagonal faces, the two different bonds and a central carbon atom. These sites were considered for a CO molecule adsorbed perpendicular with either the oxygen or the carbon atom pointing toward the surface. Because of the computational effort, only a cc-pVDZ basis was used for all atoms. The resulting one-dimensional potential energy curves on the MP2-level of theory are presented in Figure 2.

According to these results, the adsorption is preferred above the five- and six-membered rings, whereas the other adsorption sites exhibit a significantly smaller adsorption energy. The energy difference between the two ring systems is quite low, which is a consequence of the spherical shape of the C_{60} fullerene. In the rest of this paper, it will be sufficient to consider the adsorption above a six-membered ring only. With the cc-pVDZ basis set a horizontal adsorption geometry is about 3 kJ mol^{-1} less favorable. From the two perpendicular adsorption geometries the case of a carbon atom pointing toward the surface is the most stable one.

In a previous study[29] it was assumed that the carbon atom should be directed toward the longer bond, because this is less electron rich than a shorter (double) bond, therefore reducing the electrostatic repulsion to the partially negative charged carbon atom of the adsorbate. Vice versa, the oxygen atom should point toward a shorter bond. According to our results this is not the case, which can be rationalized with the very small dipole moment of CO and the minor differences between the two bond types.

It should be emphasized that on the HF and DFT (B3LYP) level the interaction is always repulsive, showing therefore the importance of dispersion interaction for this system, which is in agreement with the stronger adsorption above the five- and six-membered rings.

In this rest of this study, we will only focus on the adsorption above a hexagon with the carbon atom pointing toward the surface. For this orientation an adsorption energy of −8.5 kJ mol^{-1} has been calculated on MP2 level with a larger cc-pVTZ basis set. The equilibrium distance is 3.9 Å referred to the CO center of mass. Our result for the adsorption energy is in excellent agreement to an experimental estimation[30] giving about −8 kJ mol^{-1} . Nevertheless, this basis set (1860 basis functions) is too large to calculate a complete potential energy surface on such a high level of theory we will use it here as an internal reference standard. In the next section, model systems that reduce the computational effort will be presented.

Smaller C_{60} systems. To reduce the number of basis functions and to make the computation of higher dimensional potential energy surfaces for the electronic ground and excited state feasible, two strategies have been applied. The first was to keep all 60 atoms of the fullerene but to reduce the basis set size for those atoms that are far away from the adsorption site. The adsorption site has always been described with the cc-pVTZ basis set, while cc-pVDZ or even STO-3G has been used for the rest of the fullerene. The system class is abbreviated with **A** throughout the rest of this paper and collected in Table 1. The second approach was more drastic and consisted in the removal of some carbon atoms. The remaining fragment has been saturated with additional hydrogen atoms. We denote this system class with **B**. An prototype containing 21 carbon atoms is shown in Figure 3. As indicated, a smaller fragment of 18 carbon atoms can be constructed by removing three further atoms.

Table 1. Composition of Different Model Systems and Corresponding Number of Basis Functions, Adsorption Energies, and Equilibrium Distances

	basis[a]	no, of basis functions	E_{Ads}/kJ mol^{-1}	z/Å
ref	60 × TZ	1860	−8.5	3.9
A1	6 × TZ, 54 × DZ	996	−8.0	3.9
A2	6 × TZ, 12 × DZ, 42 × SZ	618	−5.9	3.9
A3	6 × TZ, 54 × SZ	510	−4.6	3.9
B1	21 × TZ	750	−7.6	3.8
B2	6 × TZ, 15 × DZ	510	−7.0	3.8
B3	18 × TZ	660	−7.5	3.8
B4	6 × TZ, 12 × DZ	468	−7.0	3.8

[a]TZ = cc-pVTZ, DZ = cc-pVDZ, SZ = STO-3G. The number of basis functions includes the CO atoms (always cc-pVTZ basis) as well.

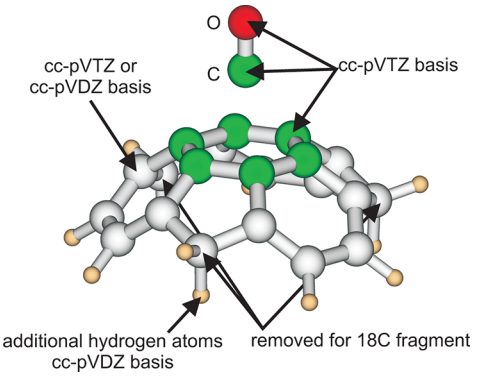

Figure 3. Fragment of 21 carbon atoms with 6 additional hydrogen atoms.

The potential energy curves for the systems **A** and **B** are presented in Figure 4 left and right, respectively.

As can been seen from Figure 4 (right), almost identical adsorption energies are obtained for 21 and 18 carbon atoms. Similarly, both energies change about 0.6 kJ mol^{-1} if most of the atoms are described by a dz basis. In spite of this convergence with system size, a large discrepancy between our

dx.doi.org/10.1021/jp305133z | J. Phys. Chem. A 2012, 116, 11211−11218

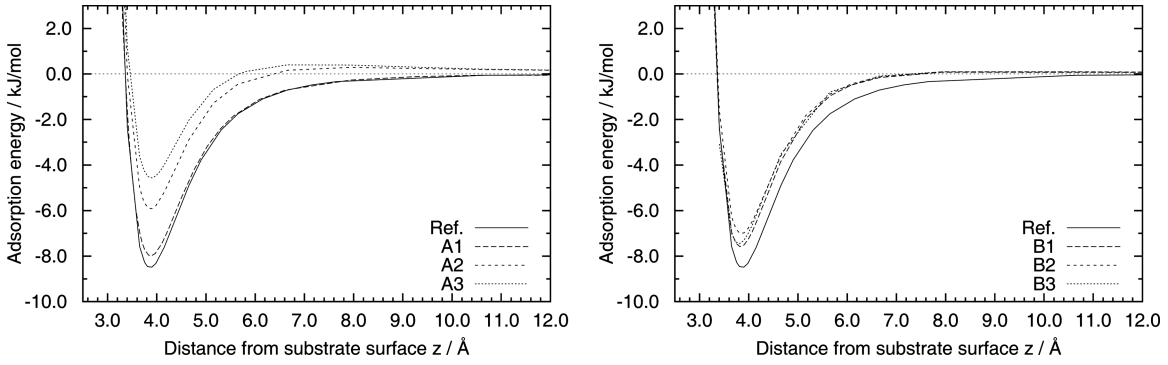

Figure 4. Adsorption energy of the CO−C_{60} system as a function of Z calculated with model **A** (left) and **B** (right).

reference system remains, implying a more fundamental reason. Furthermore, an artificial energy barrier occurs at about 8 Å (Figure 4) which is unphysical.

The same artificial barrier is found for the system class **A**, even in more pronounced fashion. In addition, the agreement with the reference system is quite poor although the number of basis functions is higher than for class **B**. This is particularly true for systems **A2** and **B4**, which have the same description of the adsorption site. A profound analysis revealed that this is a consequence of an artificial dipole moment that is extremely high for system with a minimal basis set. In these systems electron density is shifted to those atoms bearing a larger basis set. This fundamental error excludes the systems **A2** and **A3** from further studies.

Two-Dimensional Potential Energy Surface. For the two-dimensional studies the behavior at $\vartheta = 90°$ and $\vartheta = 180°$ and has been calculated as a first step. The first case corresponds to a horizontal adsorption and the latter to an oxygen above the surface. The azimuthal angle has been kept fixed at $\varphi = 0°$, which corresponds to the case shown in Figure 1. Explorative studies including this angle do not reveal any pronounced corrugation in the potential energy surface. Therefore, a two-dimensional study is sufficient. The calculated adsorption energies are display in Table 2.

Table 2. Comparison of Adsorption Energies for Some Model Systems at Different Polar Angles ϑ

ϑ/deg	A1	B3	B4	ref
0	−8.0	−7.4	−6.9	−8.5
90	−8.1	−8.4	−8.1	−8.6
180	−6.7	−6.9	−6.2	−7.5

According to the results in Figure 2 with a cc-pVDZ basis on all atoms the geometry with $\vartheta = 0°$ should be the preferred one. However, the models **A1**, **B3**, and **B3**, which worked well in the one-dimensional case, all predict a horizontal arrangement. The energy difference is quite high (1 kJ mol^{-1}) in the case of the latter two, whereas the former gives almost the same energy. Therefore, we have checked this result with our largest model of cc-pVTZ quality. These calculations (last column in Table 2) confirm the horizontal geometry and make **A1** the only reasonable system for calculating the whole potential energy surface.

The two-dimensional potential energy surface was calculated for $\vartheta = 0°, ..., 180°$ with a spacing of 10°. For each value of ϑ, 33 points at different distances were used. The other translational coordinates X and Y as well as the azimuthal angle ϕ and the interatomic distance have been kept fixed. This gave in total 627 ab initio data points that were fitted with the Levenberg−Marquardt algorithm[31] to an analytical function. The function consists of an exponential and Gaussian part for the distance Z and trigonometric functions in ϑ. It is given in eqs 4 and 5:

$$V(z) = \sum_{i=1}^{m_i} f_1 \cdot f_2 \cdot (e_1 + e_2) \tag{4}$$

with

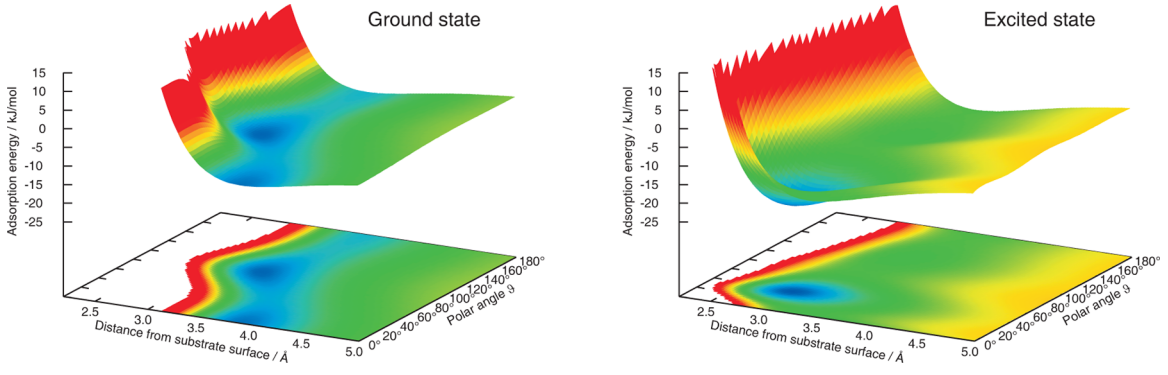

Figure 5. Adsorption energy of the CO−C_{60} system as a function of Z and ϑ calculated with model **A1** for the electronic ground (left) and an excited state (right). FC denotes the Franck−Condon point.

dx.doi.org/10.1021/jp305133z | J. Phys. Chem. A 2012, 116, 11211−11218

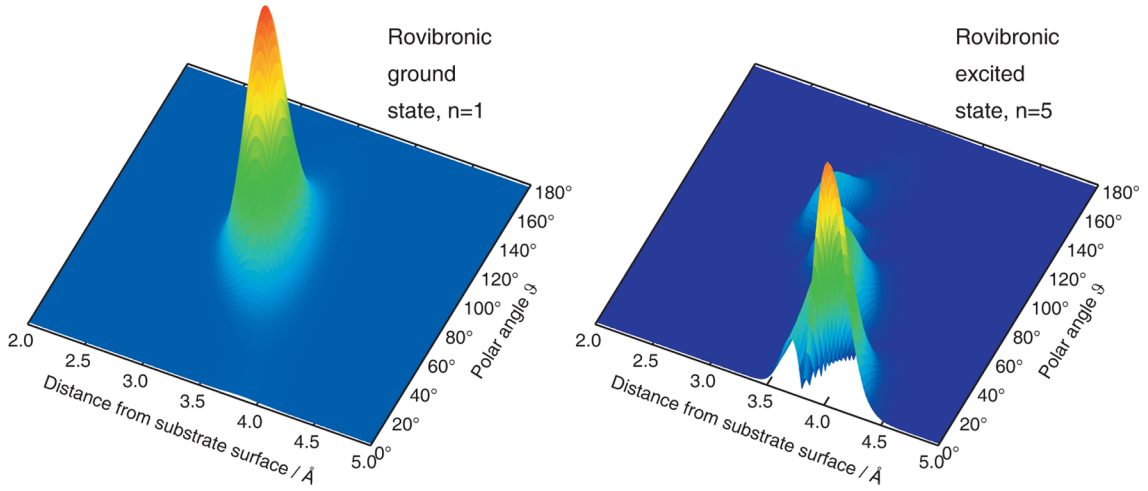

Figure 6. Probability density of the wave function for the rovibronic ground state and one selected excited state ($n = 5$) of the ground state potential energy surface.

$$f_1 = \sum_{l=0}^{m_l} a_{il} \cdot [\cos^l(\vartheta - a'_{il}) + a''^2_{il}]$$
$$f_2 = \sum_{l=0}^{m_l} b_{il} \cdot [\cos^l(\vartheta - b'_{il}) + b''^2_{il}]$$
$$e_1 = \sum_{j=1}^{m_j} c_{ij} \cdot \exp[-c'_{ij}(z - c''_{ij})]$$
$$e_1 = \sum_{j=1}^{m_j} d_{ij}^2 \cdot \exp[-d'^2_{ij}(z - d''_{ij})]^2 \quad (5)$$

and the summation running up to $m_i = 7$, $m_l = 3$, and $m_j = 1$ for the electronic ground state. The two-dimensional potential energy surface is illustrated on the left site in Figure 5. As expected from the results in Table 2, the surface is quite flat with respect to the polar angle ϑ. A global minimum occurs at $\vartheta = 90°$, $z = 3.3$ Å. However, a local minimum at $\vartheta = 0°$, $z = 3.9$ Å has almost the same adsorption energy.

Electronically Excited State. For many photodesorption processes of CO on metal oxide surfaces, it has been shown that an internal excitation of the CO molecule is the driving force.[4,6,7] The lowest excited state in the gas phase is the $\tilde{a}^3\Pi$ state that corresponds to a $5\sigma \rightarrow 2\pi^*$ transition. It is separated from the $\tilde{X}^1\Sigma^+$ ground state by 6.32 eV.[32] Although this transition is spin-forbidden in the gas phase, it can be mediated by a substrate. For the calculation the smallest possible active space comprising the 5σ-orbital and the doubly degenerate $2\pi^*$ orbitals was used. As there are two active electrons, this corresponds to a CASSCF (2,3) calculation. For a single CO molecule, the excitation energy is 6.18 eV on the CASPT2 level with a cc-pVTZ basis set. This is in reasonable agreement with the experimental findings. The same active space was used for CO adsorbed on the fullerene.

The potential energy surface of the CO–C_{60} system for this excited has been calculated on the CASPT2 level of theory. It was assumed that the BSSE is the same as at the corresponding point in the electronic ground state. This is a quite reasonable assumption and the error is comparatively small. Special care has been given to unwanted orbital rotations in the CASSCF procedure which easily occur at small distances leading to some artificial excitation of the fullerene.

The potential energy surface has been fitted according to eqs 4 and 5 with $m_i = 3$, $m_l = 2$, and $m_j = 1$ for 276 data points. The surface is depicted in the right part of Figure 5. Obviously, the global minimum is located at a polar angle of $\vartheta = 40°$ at an equilibrium distance of 2.7 Å. This is significantly shorter than in the electronic ground state and furthermore, the interaction is comparatively strong with an adsorption energy of 21.5 kJ mol^{-1}. It should be noted that in contrast to the electronic ground state there is only *one* minimum on the whole surface and its position is between the two local minima in the ground state. Therefore, a Franck–Condon excitation will lead to an interesting dynamics that will be discussed in the next section.

Quantum Dynamical Studies. As mentioned above, a starting wave packet has been obtained by imaginary time propagation. A collateral result from this procedure is the zero-point energy corrected adsorption energy. This energy is −7.4 and −20.1 kJ mol^{-1} for the ground and excited state, respectively. The density corresponding to the wave packet for the electronic ground state is visualized in Figure 6 for two rovibronic eigenstates.

To obtain correct expectation values for the desorbing molecules, the number of trajectories included in eq 3 has to be sufficiently large. The dependence of the desorption probability on the number of quantum trajectories is shown in Figure 7 together with the corresponding residence lifetimes. Both are directly connected as the temporal spacing between two trajectories is always 0.24 fs. Here, a resonance lifetime of 96 fs has been used. The desorption probability is certainly converged for 200 trajectories. For shorter resonance lifetimes the value will converge more rapidly. Therefore, 200 trajectories were used in the rest of this paper.

The resonance lifetime is the only semiempirical parameter entering our calculations. Normally, it is chosen to match the experimental desorption probability. As there are no experimental studies so far, we give the probability as a function of this lifetime in Figure 8. A range of 20–100 fs is supposed to be physically reasonable. For these values a desorption probability of 0.5% up to 12% results for the rovibronic ground state. For the fifth eigenstate (right part of Figure 8) the probability is about twice as large.

dx.doi.org/10.1021/jp305133z | J. Phys. Chem. A 2012, 116, 11211–11218

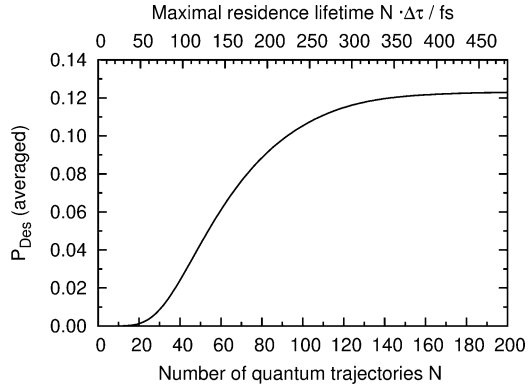

Figure 7. Desorption probability as a function of the number of quantum trajectories for a resonance lifetime of 96 fs.

Although the desorption probability is the simplest observable to detect experimentally, it does not give a profound explanation of the underlying photodesorption mechanism. After relaxation to the electronic ground state and propagating for a sufficient long time, the velocity of the desorbing molecules can be calculated. Furthermore, due to the angular gradient, the molecule is rotationally excited and the velocity can be predicted for each of these states independently. For a representative selection, these Gadzuk-averaged velocity distributions are shown in Figure 9. Here, a resonance lifetime of 96 fs has been used and the curves have been convoluted with Gaussian functions (σ = 108 ms^{-1}) to match typical experimental resolutions. In contrast to the desorption probability, these values are only slightly dependent on the resonance lifetime making the prediction independent of any empirical parameter.

Averaging over all states results in almost normally distributed velocities with a mean value of 750 ms^{-1}. The characteristics of each state, however, is quite complicated which is a consequence of the averaging scheme. For J = 14, the contribution of some trajectories is shown exemplarily in Figure 9 (right). Short residence times lead to a slow desorption channel, whereas for longer periods a faster channel of about 1300 ms^{-1} results. The shorter residence lifetimes contribute significantly due to the exponential decay in eq 3 the longer ones correspond to a higher desorption probability and represent a larger portion of the desorbing molecules. As a consequence, both channels contribute for this specific rotational state almost equivalently. Analyzing the motion of the wave packet on the excited state's potential energy surface, this motion correlates with the desorption channel: for short residence lifetimes, the wave packet spreads over all values of the polar angle ϑ and the distance to the substrates surface decreases. After about 200 fs the distance increases again and now the second desorption channel appears. In Figure 10 the probability density for two different propagation times in the excited state are given. Note how (in comparison with Figure 6 (left)) the wave packet first moves toward the surface and then moves away while its structure gets more complicated. This motion can be compared with the one-dimensional picture given by Antoniewicz and is typical for the attractive excited states. However, due to the gradients in the polar angle ϑ the desorption process cannot be fully rationalized within this picture.

The bimodal velocity distribution for these trajectories can already be found in the excited state, indicating that the velocity distribution is predominantly a consequence of the topology of the excited state's potential energy surface. Thus, there are two desorption channels that are available at different residence lifetimes (i.e., slowly desorbing molecules for short residence times, faster molecules for long residence times), resulting in a pronounced bimodality even after the Gadzuk-averaging scheme.

SUMMARY

In summary, we have simulated the laser-induced desorption of CO from a single C_{60} molecule at a high level of theory. Our results indicate that the most simple approaches to model a C_{60} molecule by using only a part of its surface fails and predicts wrong adsorption geometries and energies. Two-dimensional potential energy surfaces for the electronic ground and a representative excited state were calculated. They clearly show that different adsorption geometries occur in the electronic ground and excited state. Whereas the former prefers a horizontal orientation, the latter leads to a tilted adsorbate. The adsorption energy calculated for the electronic ground state is in good agreement with an experimental estimation.

The potential energy surfaces were subsequently used in a quantum-dynamical study. Careful analysis of the coupling of translational and rovibrational motion showed that for the rovibronic ground state a wide distribution around 750 ms^{-1} arises. However, for individual rotational quantum numbers J, the distributions exhibit a bimodal characteristics that can be traced back to the topology of the potential energy surface of the excited state. The desorption mechanism is similar to the one-dimensional case proposed by Antoniewicz.

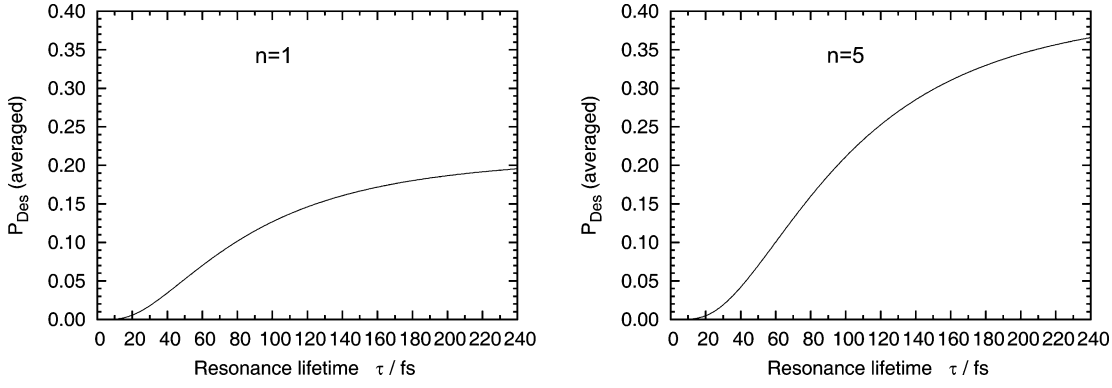

Figure 8. Desorption probability as a function of the resonance lifetime.

dx.doi.org/10.1021/jp305133z | J. Phys. Chem. A 2012, 116, 11211−11218

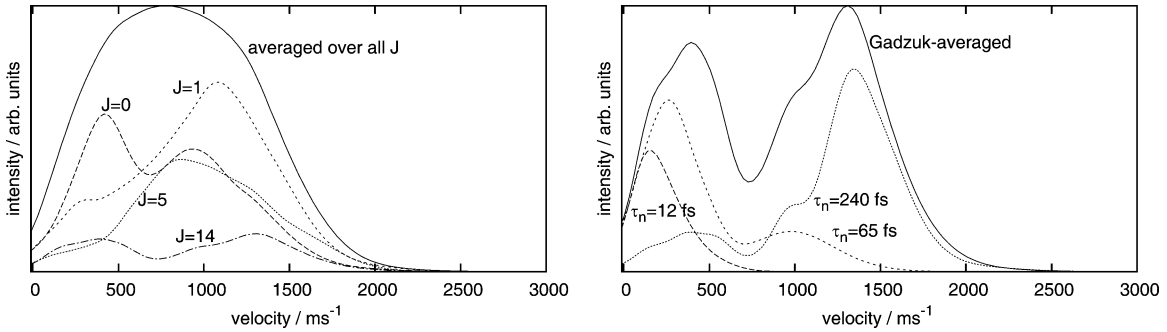

Figure 9. Gadzuk-averaged velocity distribution for different rotational quantum numbers J starting from the rovibronic ground state $n = 1$ (left) and contribution of some trajectories to the state $J = 14$. Note that the Gadzuk-averaged curves are scaled differently in both figures.

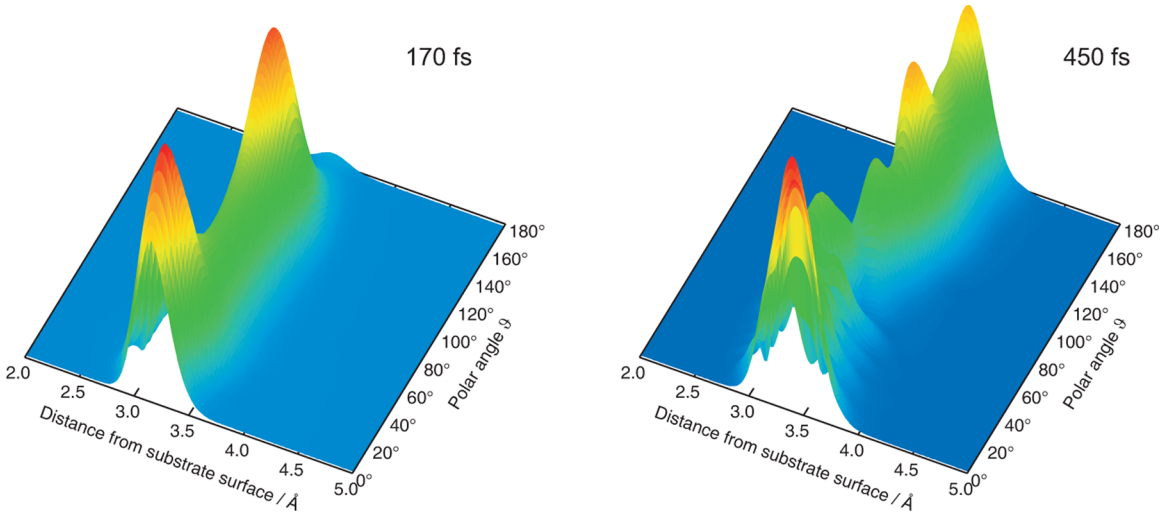

Figure 10. Probability density of the wave function for two different propagation times τ_n in the excited state.

AUTHOR INFORMATION

Corresponding Author

*E-mail: thorsten.kluener@uni-oldenburg.de.

Notes

The authors declare no competing financial interest.

REFERENCES

(1) Saalfrank, P. *Chem. Rev.* **2006**, *106*, 4116−4159.
(2) Klüner, T.; Freund, H.-J.; Freitag, J.; Staemmler, V. *J. Chem. Phys.* **1996**, *104*, 10030−10040.
(3) Thiel, S.; Pykavy, M.; Klüner, T.; Freund, H.-J.; Kosloff, R.; Staemmler, V. *Phys. Rev. Lett.* **2001**, *87*, 077601.
(4) Borowski, S.; Klüner, T.; Freund, H.-J. *J. Chem. Phys.* **2003**, *119*, 10367−10375.
(5) Koch, C. P.; Klüner, T.; Freund, H.-J.; Kosloff, R. *J. Chem. Phys.* **2003**, *119*, 1750−1765.
(6) Mehdaoui, I.; Klüner, T. *J. Phys. Chem. A* **2007**, *111*, 13233−13237.
(7) Pykavy, M.; Thiel, S.; Klüner, T. *J. Phys. Chem. B* **2002**, *106*, 12556−12562.
(8) Mehring, M.; Klüner, T. *Chem. Phys. Lett.* **2011**, *513*, 212−217.
(9) Klauda, J. B.; Jiang, J.; Sandler, S. I. *J. Phys. Chem. B* **2004**, *108*, 9842−9851.
(10) Mitschker, J.; Klüner, T. *Chem. Phys. Lett.* **2011**, *514*, 83−87.
(11) Sellgren, K.; Werner, M. W.; Ingalls, J. G.; Smith, J. D. T.; Carleton, T. M.; Joblin, C. *Astrophys. J. Lett.* **2010**, *722*, L54−L57.
(12) Goldshleger, N. F. *Fullerene Sci. Technol.* **2001**, *9*, 255−280.
(13) Dresselhaus, M. S.; Dresselhaus, G.; Eklund, P. C. *Science of fullerenes and carbon nanotubes*; Academic Press: New York, 1996.
(14) Muthu, S.; Maruthamuthu, P.; Vasudeva Rao, P. R. *Fullerene Sci. Technol.* **1993**, *1*, 481−497.
(15) Karlström, G.; Lindh, R.; Malmqvist, P.-Å.; Roos, B. O.; Ryde, U.; Veryazov, V.; Widmark, P.-O.; Cossi, M.; Schimmelpfennig, B.; Neogrady, P.; Seijo, L. *Comput. Mater. Sci.* **2003**, *28*, 222−239.
(16) Roos, B. O.; Taylor, P. R.; Siegbahn, P. E. M. *Chem. Phys.* **1980**, *48*, 157−173.
(17) Andersson, K.; Malmqvist, P. A.; Roos, B. O.; Sadlej, A. J.; Wolinski, K. *J. Phys. Chem.* **1990**, *94*, 5483−5488.
(18) Dunning, T. H., Jr. *J. Chem. Phys.* **1989**, *90*, 1007−1023.
(19) Boys, S. F.; Bernardi, F. *Mol. Phys.* **1970**, *19*, 553−566.
(20) Gadzuk, J. W.; Richter, L. J.; Buntin, S. A.; King, D. S.; Cavanagh, R. R. *Surf. Sci.* **1990**, *235*, 317−333.
(21) Menzel, D.; Gomer, R. *J. Chem. Phys.* **1964**, *41*, 3311−3328.
(22) Antoniewicz, P. R. *Phys. Rev. B* **1980**, *21*, 3811−3815.
(23) Saalfrank, P. *Chem. Phys.* **1996**, *211*, 265−276.
(24) Heather, R.; Metiu, H. *J. Chem. Phys.* **1987**, *86*, 5009−5017.
(25) Feit, M. D.; Fleck, J. A., Jr. *J. Chem. Phys.* **1983**, *78*, 301−308.
(26) Kosloff, R.; Tal-Ezer, H. *Chem. Phys. Lett.* **1986**, *127*, 223−230.
(27) Frisch, M. J.; et al. *Gaussian 03*, Revision D.02; Gaussian, Inc.: Wallingford, CT, 2004.
(28) Hedberg, K.; Hedberg, L.; Bethune, D. S.; Brown, C. A.; Dorn, H. C.; Johnson, R. D.; de Vries, M. *Science* **1991**, *254*, 410−412.
(29) van Smaalen, S.; Dinnebier, R.; Holleman, I.; von Helden, G.; Meijer, G. *Phys. Rev. B* **1998**, *57*, 6321−6324.
(30) Fastow, M.; Kozirovski, Y.; Folman, M. *Surf. Sci.* **1995**, *331*−*333*, 121−126.
(31) Press, W.; Teukolsky, S.; Vetterling, W.; Flannery, B. *Numerical recipes in FORTRAN: The art of scientific computing*, 2nd ed.; Cambridge University Press: Cambridge, U.K., 1992.

(32) Nielsen, E. S.; Jørgensen, P.; Oddershede, J. *J. Chem. Phys.* **1980**, *73*, 6238−6246.